



**Structural and Electrical Properties of Garnet-type
Structure $\text{Li}_7\text{La}_3\text{Ce}_2\text{O}_{12}$ as Solid Electrolytes for Solid-
state Li-ion Batteries**

by

**Nazerah Binti Yaacob
(2030413149)**

A thesis submitted in fulfillment of the requirements for the degree of
Master of Science in Materials Engineering

**Faculty of Chemical Engineering Technology
UNIVERSITI MALAYSIA PERLIS**

2022

ACKNOWLEDGEMENT

All the praises and thanks to Allah S. W. T. This thesis would not have been possible without the guidance of my supervisor and lecturers, help from friends and support from family.

First and foremost, I would like to express my deepest and sincere gratitude to my main supervisor Assoc. Prof. Dr. Mohd Sobri Idris for his constant excellent guidance, commitment and encouragement throughout the whole period of my master's research studies. He has been a great supervisor who always likes to share his knowledge, especially in X-ray diffraction and Rietveld Refinement. He provided me with a conducive atmosphere for research activity and had a great experience developing myself with confidence through interesting discussion/group meetings. I am very grateful for his patience and the motivation he has given during the learning process. My research would not have been possible without his support. Thank you to my co-supervisor Dr. Salmie Suhana Che Abdullah for her advice and guidance. I am also very thankful for the valuable knowledge and experience that Assoc. Prof. Ir. Ts Dr. Rozana Aina Maulat Osman shared. She has inspired me to learn more about electrical knowledge.

Secondly, I would like to thank every member of the Centre of Excellence Frontier Materials Research, particularly Dr. Ku Noor Dhaniah, who has been supportive, caring and always guide me to the best of her knowledge. My Master's studies would not be possible and run smoothly without her support. Thanks to my fellow friends Adlina and Nadia, who shared the same journey that always supported each other.

In addition, I am thankful to the Ministry of Higher Education (MOHE) Malaysia for funding this project through the Fundamental Research Grant Scheme 2019 (FRGS Grant No.: FRGS/1/2019/TK05/UNIMAP/02/14)

Finally, I would like to thank my family members for the encouragement, love and support throughout this journey. My deepest gratitude goes to my parents for giving me the strength to complete my studies. This thesis is dedicated to you.

TABLE OF CONTENTS

	PAGE
DECLARATION OF THESIS	i
ACKNOWLEDGEMENT	ii
TABLE OF CONTENTS	iii
LIST OF TABLES	vi
LIST OF FIGURES	vii
LIST OF ABBREVIATIONS	xii
LIST OF SYMBOLS	xiii
ABSTRAK	xiv
ABSTRACT	xv
CHAPTER 1 : INTRODUCTION	1
1.1 Background of Li-ion Batteries	1
1.1.1 Anode (Negative Electrodes)	4
1.1.2 Cathode (Positive Electrodes)	4
1.1.3 Electrolytes	5
1.1.4 Mechanism of Charge-discharge Li-ion Batteries	5
1.2 Problem Statement	7
1.3 Research Objectives	8
1.4 Scope of Study	9
1.5 Thesis Structure	9
CHAPTER 2 : LITERATURE REVIEW	11
2.1 Introduction	11

2.2	Solid-state Li-ion Batteries	11
2.3	Solid Electrolytes of Li-ion Batteries	13
2.3.1	Sulfide-types solid electrolytes	15
2.3.2	Oxide-types solid electrolytes	16
2.4	Oxide-types Solid Electrolytes	17
2.4.1	Sodium Superionic Conductor (NASICON)	17
2.4.2	Lithium Superionic Conductor (LISICON)	20
2.4.3	Perovskite-type Structure	22
2.4.4	Garnet-type Structure	25
2.5	Histry of Garnet-type Structure $\text{Li}_7\text{La}_3\text{Zr}_2\text{O}_{12}$ as Solid Electrolytes	27
2.6	Impedance Spectroscopy Characterization	33
CHAPTER 3 : METHODOLOGY		42
3.1	Introduction	42
3.2	Materials Synthesis	42
3.3	Materials Characterization	46
3.3.1	Powder X-ray Diffraction	46
3.3.2	Impedance Spectroscopy	48
3.3.3	Scanning Electron Microscopy	51
CHAPTER 4 : RESULTS & DISCUSSION		52
4.1	Introduction	52
4.2	Characterization of $\text{Li}_7\text{La}_3\text{Ce}_2\text{O}_{12}$ prepared using conventional solid-state reaction routes	52
4.2.1	X-ray Diffraction Analysis of $\text{Li}_7\text{La}_3\text{Ce}_2\text{O}_{12}$	53
4.2.2	Electrical Properties of $\text{Li}_7\text{La}_3\text{Ce}_2\text{O}_{12}$	60
4.2.3	Scanning Electron Microscopy Analysis on $\text{Li}_7\text{La}_3\text{Ce}_2\text{O}_{12}$	67
4.3	The Effect of Lithium Excess on $\text{Li}_7\text{La}_3\text{Ce}_2\text{O}_{12}$	69

4.3.1	X-ray Diffraction Analysis on the Effect of Lithium Excess of $\text{Li}_7\text{La}_3\text{Ce}_2\text{O}_{12}$	69
4.3.2	Electrical Properties on the Effect of Lithium Excess of $\text{Li}_7\text{La}_3\text{Ce}_2\text{O}_{12}$	71
4.3.3	Scanning Electron Microscopy Analysis on the Effect of Lithium Excess of $\text{Li}_7\text{La}_3\text{Ce}_2\text{O}_{12}$	79
4.4	The Effect of Different Mixing Condition of $\text{Li}_7\text{La}_3\text{Ce}_2\text{O}_{12}$	82
4.4.1	X-ray Diffraction Analysis of $\text{Li}_7\text{La}_3\text{Ce}_2\text{O}_{12}$ with Different Mixing Condition	82
4.4.2	Electrical Properties of $\text{Li}_7\text{La}_3\text{Ce}_2\text{O}_{12}$ with Different Mixing Condition	84
4.4.3	Scanning Electron Microscopy analysis of $\text{Li}_7\text{La}_3\text{Ce}_2\text{O}_{12}$ with Different Mixing Condition	90
4.5	Preliminary Study on Sn and Zr doped $\text{Li}_7\text{La}_3\text{Ce}_2\text{O}_{12}$	92
4.5.1	X-ray diffraction Analysis on Sn and Zr doped $\text{Li}_7\text{La}_3\text{Ce}_2\text{O}_{12}$	92
4.5.2	Electrical Properties of Sn and Zr doped $\text{Li}_7\text{La}_3\text{Ce}_2\text{O}_{12}$	93
4.5.3	The Scanning Electron Microscopy analysis on Sn and Zr doped $\text{Li}_7\text{La}_3\text{Ce}_2\text{O}_{12}$	100
CHAPTER 5 : CONCLUSION		103
5.1	Conclusions	103
5.2	Future Outlook	105
REFERENCES		106
APPENDIX A SUPPORTING DATA		113
APPENDIX B CALCULATION FOR MASS OF RAW MATERIALS		115
LIST OF PUBLICATIONS		116

LIST OF TABLES

	PAGE
Table 2.1	Summary of properties of solid electrolytes. 27
Table 2.2	Capacitance and their possible interpretation (Irvine et al., 1990). 37
Table 2.3	Typical values of ionic conductivity (West, 2003). 39
Table 3.1	The specifications for the preparation of the samples. 44
Table 4.1	The initial structure model of $\text{Li}_7\text{La}_3\text{Ce}_2\text{O}_{12}$ from ICSD data (#65548). 58
Table 4.2	Refined structure model for $\text{Li}_7\text{La}_3\text{Ce}_2\text{O}_{12}$ prepared at 900 °C. 59
Table 4.3	The fitting data for $\text{Li}_7\text{La}_3\text{Ce}_2\text{O}_{12}$ sample at selected temperature. 63
Table 4.4	The fitting data for $\text{Li}_7\text{La}_3\text{Ce}_2\text{O}_{12}$ with different amount of lithium excess sample at selected temperature. 74
Table 4.5	The fitting data for $\text{Li}_7\text{La}_3\text{Ce}_2\text{O}_{12}$ with different processing condition at 180 °C. 86
Table 4.6	Summary of <i>dc</i> conductivities at different temperature for $\text{Li}_7\text{La}_3\text{Ce}_2\text{O}_{12}$ with different preparation method. 88
Table 4.7	The fitting data for $\text{Li}_7\text{La}_3\text{Ce}_2\text{O}_{12}$ with Sn and Zr-doped at 180 °C. 96
Table 4.8	Summary of conductivity data for $\text{Li}_7\text{La}_3\text{Ce}_2\text{O}_{12}$ at 300 °C. 102

LIST OF FIGURES

	PAGE	
Figure 1.1	Diagram of energy density and specific density for various types of batteries (Kim et al., 2015).	3
Figure 1.2	Charging and discharging mechanism of Li-ion batteries.	6
Figure 1.3	Schematic diagram of conventional and solid-state Li-ion batteries.	7
Figure 2.1	The performance of different solid electrolytes (Manthiram, Yu, and Wang 2017).	14
Figure 2.2	Crystal structure of NASICON-types solid electrolytes (Sebastian & Gopalakrishnan, 2003).	20
Figure 2.3	Crystal structure of perovskite-type structure solid electrolytes $\text{Li}_{3x}\text{La}_{2/3x}\text{TiO}_3$ (Stramare, Thangadurai & Weppner, 2003).	22
Figure 2.4	Crystal structure of tetragonal $\text{Li}_7\text{La}_3\text{Zr}_2\text{O}_{12}$. (Awaka, Kijima, Hayakawa & Akimoto, 2009).	28
Figure 2.5	(a) Crystal structure of cubic $\text{Li}_7\text{La}_3\text{Zr}_2\text{O}_{12}$; (b) Coordination of polyhedra around the Li_1 and Li_2 (Aleksandrov et al., 2020).	29
Figure 2.6	The diagram of (a) equivalent circuit and (b) complex impedance of two electrolytes and electrode effect denoted as R_b , R_g , and R_e represented as bulk, grain boundary and electrode respectively.	35
Figure 2.7	The non-ideal response of bulk component for $\text{Ba}_2\text{TiSi}_2\text{O}_8$ (Osman & Idris, 2013).	36

Figure 2.8	The homogeneous materials with coincide peaks at lower frequency scale of Z''/M'' spectroscopic plot (Sinclair, 1995).	38
Figure 2.9	The example of Z''/M'' spectroscopic plot for inhomogeneous sample (Yang Liu, West & Trolier-McKinstry, 2013).	38
Figure 2.10	The (a) first universalities and (b) second universalities of conductivity as a frequency (Funke et al. 2010).	40
Figure 2.11	The frequency-dependence of the conductivity of α -alumina (Almond & West, 1983).	41
Figure 3.1	The flow chart of the research methodology.	45
Figure 3.2	The X-ray diffraction experiment.	47
Figure 3.3	The derivation of Bragg's Law.	48
Figure 3.4	The schematic diagram of impedance spectroscopy analysis.	51
Figure 4.1	XRD pattern for $\text{Li}_7\text{La}_3\text{Ce}_2\text{O}_{12}$ heating at 600 °C and 700 °C compared to a database.	54
Figure 4.2	XRD pattern for $\text{Li}_7\text{La}_3\text{Ce}_2\text{O}_{12}$ heating at 800 °C and 900 °C compared to a database.	55
Figure 4.3	The X-ray diffraction pattern of $\text{Li}_7\text{La}_3\text{Ce}_2\text{O}_{12}$ compared with the database.	56
Figure 4.4	Rietveld refinement profile of the $\text{Li}_7\text{La}_3\text{Ce}_2\text{O}_{12}$	58
Figure 4.5	The crystal structure of garnet-type $\text{Li}_7\text{La}_3\text{Ce}_2\text{O}_{12}$ drawn by using computer software, VESTA.	59
Figure 4.6	Complex impedance plot of $\text{Li}_7\text{La}_3\text{Ce}_2\text{O}_{12}$ at different temperatures.	62

Figure 4.7	The fitted data of Cole – Cole plot Z' versus Z'' at selected temperature 210 °C, 240 °C, 270 °C and 300 °C.	63
Figure 4.8	The electrical conductivity as a function of the frequency of $\text{Li}_7\text{La}_3\text{Ce}_2\text{O}_{12}$ between 30 °C and 300 °C.	65
Figure 4.9	The temperature dependence of total conductivity for $\text{Li}_7\text{La}_3\text{Ce}_2\text{O}_{12}$.	67
Figure 4.10	The SEM images of $\text{Li}_7\text{La}_3\text{Ce}_2\text{O}_{12}$.	68
Figure 4.11	(a) The XRD patterns of $\text{Li}_7\text{La}_3\text{Ce}_2\text{O}_{12}$ at temperature 800 °C with different lithium excess, (b) The enlargement of the peak	70
Figure 4.12	(a) The XRD patterns of $\text{Li}_7\text{La}_3\text{Ce}_2\text{O}_{12}$ at temperature 900 °C with different amount of lithium excess, (b) The enlarged diffraction data between $2\theta = 31$ and 32° .	71
Figure 4.13	Complex impedance plot of $\text{Li}_7\text{La}_3\text{Ce}_2\text{O}_{12}$ with different amount of lithium excess (a) 10%, (b) 20%, (c) 30% and (d) 40% at different temperatures.	72
Figure 4.14	The fitted data of Cole – Cole plot Z' versus Z'' at (a) 150 °C, (b) 160 °C, (c) 180 °C and (d) 190 °C for (a) 10%, (b) 20%, (c) 30% and (d) 40% lithium excess, respectively.	73
Figure 4.15	Capacitance of $\text{Li}_7\text{La}_3\text{Ce}_2\text{O}_{12}$ with different amount of lithium excess as (a) 10%, (b) 20%, (c) 30% and (d) 40% as a function of frequency at different temperatures.	75
Figure 4.16	The Z'' / M'' spectroscopy plot for $\text{Li}_7\text{La}_3\text{Ce}_2\text{O}_{12}$ with different amount of lithium excess (a) 10%, (b) 20%, (c) 30% and (d) 40% at different temperatures.	76
Figure 4.17	The conductivity of the $\text{Li}_7\text{La}_3\text{Ce}_2\text{O}_{12}$ with different amounts of lithium excess at temperature 300 °C.	78

Figure 4.18	The Arrhenius plot of activation energy on $\text{Li}_7\text{La}_3\text{Ce}_2\text{O}_{12}$ with 10%, 20%, 30% and 40% amount lithium excess at frequency 1 kHz.	79
Figure 4.19	The SEM images of $\text{Li}_7\text{La}_3\text{Ce}_2\text{O}_{12}$ with (a) 10%, (b) 20%, (c) 30% and (d) 40% amount lithium excess.	81
Figure 4.20	The X-ray diffraction pattern of $\text{Li}_7\text{La}_3\text{Ce}_2\text{O}_{12}$ samples prepared with different synthesizing routes at temperature 900 °C.	83
Figure 4.21	The (a) complex impedance plot, (b) capacitance plot and (c) Z'' / M'' spectroscopy plot of $\text{Li}_7\text{La}_3\text{Ce}_2\text{O}_{12}$ samples prepared with different synthesizing routes at temperature 180 °C.	85
Figure 4.22	The fitted data of Cole – Cole plot Z' versus Z'' with different processing condition using (a) pestle and mortar and (b) ball-milling at 180 °C.	86
Figure 4.23	The conductivity as a function of frequency of $\text{Li}_7\text{La}_3\text{Ce}_2\text{O}_{12}$ prepared with different synthesizing routes at temperature 300 °C.	88
Figure 4.24	The Arrhenius plot for $\text{Li}_7\text{La}_3\text{Ce}_2\text{O}_{12}$ prepared with different synthesizing routes at a temperature range from 80 °C to 300 °C at 1 kHz.	90
Figure 4.25	The SEM images for both $\text{Li}_7\text{La}_3\text{Ce}_2\text{O}_{12}$ samples prepared by using (a) pestle and mortar and (b) planetary ball-mill method sintered at 900 °C.	91
Figure 4.26	The X-ray diffraction pattern for Sn and Zr doped $\text{Li}_7\text{La}_3\text{Ce}_2\text{O}_{12}$ at temperature 900 °C.	93
Figure 4.27	The (a) complex impedance plot, (b) capacitance plot and (c) Z'' / M'' spectroscopy plot of $\text{Li}_7\text{La}_3\text{Ce}_2\text{O}_{12}$ samples with Sn and Zr doped measured at temperature 180 °C.	95

Figure 4.28	The fitted data of Cole – Cole plot Z' versus Z'' with different doping element (a) Sn-doped and (b) Zr-doped at 180 °C.	96
Figure 4.29	The conductivity as a function of frequency for (a) Sn-doped and (b) Zr-doped $\text{Li}_7\text{La}_3\text{Ce}_2\text{O}_{12}$ at temperature in the range of 30 °C to 300 °C.	98
Figure 4.30	The conductivity as a function of the frequency of Sn and Zr-doped $\text{Li}_7\text{La}_3\text{Ce}_2\text{O}_{12}$ at different temperatures.	98
Figure 4.31	The activation energy plot for $\text{Li}_7\text{La}_3\text{Ce}_2\text{O}_{12}$ sample doped with Sn and Zr at temperature between 80 °C and 300 °C at frequency 1 kHz.	100
Figure 4.32	The SEM images of (a) Sn-doped and (b) Zr-doped $\text{Li}_7\text{La}_3\text{Ce}_2\text{O}_{12}$ sintered at 900 °C for 12 hours.	101

LIST OF ABBREVIATIONS

IS	Impedance spectroscopy
LISICON	Lithium superionic conductor
LLTO	Lithium lanthanum titanate
LSTH	Lithium strontium titanate hafnate
LSTZ	Lithium strontium titanate zirconate
NASICON	Sodium superionic conductor
SEM	Scanning electron microscope
XRD	X-ray diffraction

©This item is protected by original copyright

LIST OF SYMBOLS

a	Lattice a
A	Electrode area
b	Lattice b
c	Lattice c
C	Capacitance
$^{\circ}\text{C}$	Degree Celsius
d	Interplanar spacing
eV	Electron volt
E_a	Activation energy
f	Frequency
F	Farad
K	Boltzmann's constant
l	Electrode separation
R	Resistance
T	Absolute temperature
Z'	Real part of Impedance
Z''	Imaginary part of Impedance
ϵ_o	Dielectric constant in vacuum
ϵ_r	Relative dielectric constant
σ	Conductivity
σ_o	Pre-exponential factor
σ_{dc}	DC conductivity
θ	Diffraction angle
λ	Wavelength of X-rays
ρ	Resistivity
ω	Angular frequency

Struktur dan Sifat Elektrik bagi $\text{Li}_7\text{La}_3\text{Ce}_2\text{O}_{12}$ yang Berstruktur Jenis Garnet sebagai Elektrolit Pepejal bagi Bateri Li-ion Berkeadaan Pepejal

ABSTRAK

Perkembangan teknologi pada masa kini mendorong peningkatan keperluan bateri boleh dicas semula yang mempunyai prestasi yang unggul dan selamat digunakan. Masalah keselamatan bateri Li-ion konvensional menjadi pendorong untuk mengembangkan bateri Li-ion berkeadaan pepejal di mana elektrolit cair digantikan dengan bahan elektrolit pepejal. Banyak jenis elektrolit pepejal telah diselidiki secara terperinci dalam beberapa tahun kebelakangan dan struktur jenis garnet adalah elektrolit pepejal yang terbaik. Oleh itu, kerja ini dimulakan untuk mengkaji struktur jenis garnet $\text{Li}_7\text{La}_3\text{Ce}_2\text{O}_{12}$ sebagai calon berpotensi untuk elektrolit pepejal dalam bateri Li-ion berkeadaan pepejal. Struktur, sifat elektrik dan sifat mikrostruktur $\text{Li}_7\text{La}_3\text{Ce}_2\text{O}_{12}$ dikaji secara sistematik. Sampel disintesis menggunakan kaedah tindak balas keadaan pepejal konvensional pada suhu $600\text{ }^\circ\text{C}$ - $900\text{ }^\circ\text{C}$ di udara selama 12 jam. Komposisi ini dicirikan dengan menggunakan teknik-teknik Pembelauan sinar-X (XRD), Analisis Impedans Spektroskopi (IS) dan Mikroskop Imbasan Elektron (SEM). Penyelidikan ini melibatkan tiga penyiasatan utama. Pertama, kajian ini dimulakan dengan menilai fasa tulen $\text{Li}_7\text{La}_3\text{Ce}_2\text{O}_{12}$ dan kestabilan struktur hablurnya hingga $900\text{ }^\circ\text{C}$. Semua corak XRD dapat diindeks dengan struktur tetragonal dan kumpulan ruang $I4/mmm$. Sifat elektrik menunjukkan bahawa $\text{Li}_7\text{La}_3\text{Ce}_2\text{O}_{12}$ menunjukkan dataran tinggi frekuensi dengan penyebaran di kawasan frekuensi tinggi pada plot kekonduksian yang menunjukkan sifat elektrolit pepejal. Walaupun begitu, kekonduksian dianggap rendah sekitar $4.07 \times 10^{-6}\text{ S cm}^{-1}$ pada $300\text{ }^\circ\text{C}$ diukur pada 1 kHz . Di samping itu, ia menunjukkan ukuran butiran kecil dengan sejumlah besar liang yang mungkin menyumbang kepada kekonduksian yang rendah. Oleh itu, kajian lanjutan dilakukan terhadap implikasi kekonduksian $\text{Li}_7\text{La}_3\text{Ce}_2\text{O}_{12}$ dengan menggunakan jumlah tambahan litium yang berbeza: 10%, 20%, 30% dan 40%. Hasil kajian menunjukkan bahawa kekonduksian $\text{Li}_7\text{La}_3\text{Ce}_2\text{O}_{12}$ menjadi lebih tinggi iaitu $7.14 \times 10^{-6}\text{ S cm}^{-1}$ dengan menggunakan jumlah tambahan litium sebanyak 30%. Selanjutnya, diperhatikan melalui struktur mikro, ukuran saiz butir menjadi lebih besar berukuran $26\text{ }\mu\text{m}$. Oleh kerana kaedah pemrosesan mempengaruhi sifat-sifat bahan seramik, perbandingan terhadap kesan penggunaan kaedah lesung penumbuk dan pengisar bola planet semasa penyediaan telah dikaji. Hasil kajian yang mengejutkan di mana $\text{Li}_7\text{La}_3\text{Ce}_2\text{O}_{12}$ yang disediakan menggunakan lesung penumbuk mempunyai sifat yang lebih baik dibandingkan dengan sampel yang disediakan menggunakan kaedah pengisar bola planet. Kekonduksian sampel yang disediakan menggunakan lesung penumbuk lebih tinggi sedikit dan mempunyai butiran biji yang bersambung dengan baik. Sebaliknya, sampel yang disediakan menggunakan pengisar bola planet menunjukkan butiran yang kurang bersambung dengan sejumlah besar liang yang mencerminkan kekonduksian sampel yang rendah. Kesimpulannya, elektrolit pepejal $\text{Li}_7\text{La}_3\text{Ce}_2\text{O}_{12}$ yang disediakan menggunakan kaedah lesung penumbuk dengan tambahan jumlah litium sebanyak 30% mempunyai ciri-ciri yang terbaik berbanding yang lain. Elektrolit pepejal $\text{Li}_7\text{La}_3\text{Ce}_2\text{O}_{12}$ berpotensi digunakan dalam aplikasi bateri bersuhu tinggi kerana kekonduksian yang tinggi tercapai pada suhu yang tinggi.

Structural and Electrical Properties of Garnet-type Structure $\text{Li}_7\text{La}_3\text{Ce}_2\text{O}_{12}$ as Solid Electrolytes for Solid-state Li-ion Batteries

ABSTRACT

Technology development nowadays leads to a growing need for rechargeable batteries with superior performance and are safe to be used. The safety issues of conventional Li-ion batteries become a driving force for developing solid-state Li-ion batteries where liquid electrolytes were replaced with solid electrolytes materials. Many types of solid electrolytes have been investigated in detail in the past years and garnet-type structure is the most promising solid electrolyte. Hence, this work is embarked to study the garnet-type structure $\text{Li}_7\text{La}_3\text{Ce}_2\text{O}_{12}$ as potential candidates for solid electrolytes in solid-state Li-ion batteries. The structural, electrical properties and microstructure properties of $\text{Li}_7\text{La}_3\text{Ce}_2\text{O}_{12}$ were systematically studied. The samples were synthesized using a conventional solid-state reaction method at temperature $600\text{ }^\circ\text{C} - 900\text{ }^\circ\text{C}$ in the air for 12 hours. These compositions were characterized by using X-ray Diffraction (XRD), Impedance Spectroscopy (IS) and Scanning Electron Microscopy (SEM) techniques. This research involves three main investigations. Firstly, the study was initiated by evaluating the purity phase of $\text{Li}_7\text{La}_3\text{Ce}_2\text{O}_{12}$ and structural stability up to $900\text{ }^\circ\text{C}$. All the XRD patterns could be indexed with the tetragonal structure and the space group of $I4/mmm$. The electrical properties revealed that $\text{Li}_7\text{La}_3\text{Ce}_2\text{O}_{12}$ exhibits frequency plateau with a dispersion at high frequency region in the conductivity plot indicating solid electrolytes' properties. Nevertheless, the conductivity is considered low which is about $4.07 \times 10^{-6}\text{ S cm}^{-1}$ at $300\text{ }^\circ\text{C}$ measured at 1 kHz. In addition, it exhibits a small grain size with a large number of pores that might be contributed to low conductivity. Hence, further study was conducted with different amounts of lithium excess: 10%, 20%, 30% and 40% in order to enhance the conductivity of $\text{Li}_7\text{La}_3\text{Ce}_2\text{O}_{12}$. The results showed that $\text{Li}_7\text{La}_3\text{Ce}_2\text{O}_{12}$ exhibited a relatively higher conductivity of $7.14 \times 10^{-6}\text{ S cm}^{-1}$ with 30% amount of lithium excess. Furthermore, the microstructure was observed with a larger grain size without any pores. Since the processing method affects the properties of ceramic materials, therefore the comparison between $\text{Li}_7\text{La}_3\text{Ce}_2\text{O}_{12}$ was prepared using pestle mortar and planetary ball-mill method. The properties of both samples were compared. Surprisingly, $\text{Li}_7\text{La}_3\text{Ce}_2\text{O}_{12}$ prepared using pestle mortar has better properties than the sample prepared using the planetary ball-mill method. Samples that used pestle mortar exhibited slightly higher conductivities with well-connected grain. But the sample that was prepared using a planetary ball-mill exhibited poorly connected grain with a large number of pores observed that might contribute to the low conductivity. It can be summarized that $\text{Li}_7\text{La}_3\text{Ce}_2\text{O}_{12}$ prepared using pestle and mortar with 30% as the optimum amount of lithium excess exhibit the best properties compared to others. Since the high conductivity achieved at high temperature, the solid electrolytes $\text{Li}_7\text{La}_3\text{Ce}_2\text{O}_{12}$ potentially can be used for high temperature battery application.

CHAPTER 1 : INTRODUCTION

1.1 Background of Li-ion Batteries

The world's demand for limited natural resources becomes a significant concern since the energy crisis happens. Natural resources are decreasing day by day as they are used to power industrial society. It is commonly non-renewable energy such as fossil fuel, minerals and metal ores are expected to decline. There is a limited supply of these natural resources. It may take over a century or thousands of years to replenish the stores while naturally occurring. Governments and individuals involved are prioritizing the use of renewable resources and enhanced conservation of the uncontrolled use of natural assets. Recently, the production of alternative green (zero emissions) energy storage and conversion devices such as batteries and solar cells has become increasingly important. Batteries can be fully self-contained and do not need any chemical input or export, unlike fuel cells requiring constant fuel supply (Thangadurai, Narayanan & Pinzaru, 2014).

Consequently, the demand for batteries recently gives high interest. Batteries can be classified into two categories which are primary battery and secondary battery. A primary battery is a non-rechargeable and single used battery—for example, dry cells (most alkaline batteries). In contrast, a secondary battery is a battery that can be recharged after being used, for example, nickel-cadmium (NiCd), nickel-metal hydride (NiMH), Lithium-ion (Li-ion) batteries and lead-acid batteries (Nishi, 2014). Among these types of rechargeable batteries, the most popular is Li-ion batteries. It has outstanding properties compared to other conventional secondary batteries, including Ni-Cd, NiMH, and lead-acid batteries.

In the year 1978, Whittingham discovered the development of intercalation electrodes (Whittingham, 1978). The discovery initially focused on the cathode side, where the materials can reversibly accept and release Li-ion in and out from its structure to balance the positive charge of the inserted Li-ion without having a lattice collapse. Later on, the first Li-ion cathode materials were discovered by Goodenough in 1980, where lithium cobalt oxide, LiCoO_2 become the most promising cathode material (Mizushima, Jones, Wiseman & Goodenough, 1980).

Along with this fundamental discovery, the first commercialization of secondary Li-ion batteries was achieved by Japanese Sony manufacturers in 1991 (Yoshino, 2014). The Sony battery successfully provides a proper electrode where graphite act as the anode and LiCoO_2 act as the cathode. Anode graphite was able to accept the Li-ion during discharging while LiCoO_2 cathode capable of providing Li-ions, able to release and accept back Li-ions in the reversible matter to assure the battery's life.

The technological revolution leads to a growing need for rechargeable batteries with greater capacity or with reduced size and weight for a given capacity. Li-ion battery is a type of rechargeable battery that reversible chemical reactions happen in both directions through the charging and discharging process. The outstanding properties of Li-ion batteries provide excellent features were (i) high operating voltage (3.7 V on the average), (ii) high gravimetric and volumetric energy densities, (iii) no memory effect, (iv) low self-discharge rate (less than 20% per year) and (v) operates in a wide range of temperature (Nishi, 2014).

In addition, the Li-ion batteries also provide a large amount of current, lighter than comparable batteries of other types, produce a nearly constant voltage as they discharge and slowly lose their charge when stored. Figure 1.1 illustrated the gravimetric and volumetric energy densities for conventional batteries, which shows Li-ion batteries possess high energy density values and are lightweight which satisfactorily serve the evolving technology.

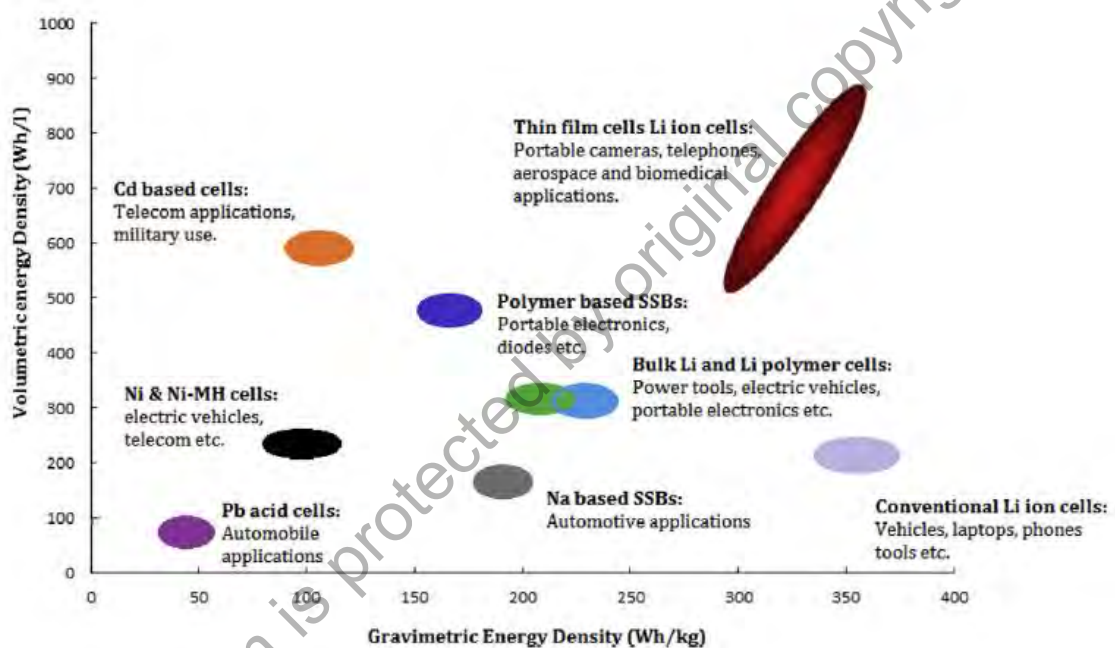


Figure 1.1 Diagram of energy density and specific density for various types of batteries (Kim et al., 2015).

Therefore, the development of technology nowadays increases with the demand for Li-ion batteries. Li-ion batteries are widely used as power sources for hand-held electronic devices such as mobile phones, laptop computers, digital cameras and other electronic devices due to higher energy density, lightweight, longer lifespan and environmentally friendliness. Generally, Li-ion batteries mainly consist of anode, cathode and electrolyte.

1.1.1 Anode (Negative Electrodes)

An anode is a negatively charged electrode by which the Li-ion intercalates in charging and deintercalation in discharging process while electrons leave an electrical device. An anode is a potentially good material that can store Li/Li⁺ to great capacity in Li-ion batteries (Kim et al., 2015). Commonly, graphite was used as the anode material since it has superior discharge capacity. In addition, Li metal alloys also provide a much higher capacity than graphite. However, the significant expansion and contraction of volume during the charging-discharging process becomes a severe drawback of these materials. Examples of materials used as an anode are lithium-based metal oxide, graphite, and carbon-based materials.

1.1.2 Cathode (Positive Electrodes)

A cathode is a positively charged electrode which is one of the crucial components in the solid-state Li-ion batteries and it must be structurally stable. The cathode is important in solid-state Li-ion batteries as it supplies the battery with the necessary ions during the charging and discharging process (Whittingham, 2004). Since the charging-discharging process involves transference or movement of ions across, it is crucial that the ionic conductivity of the cathode must be good. The material widely used as cathode material is LiCoO₂, as it exhibits a layered structure that is suitable for the lithiation and delithiation process. It also has a relatively high specific energy of about 150 mAh g⁻¹. In addition, lithium manganese oxide (LiMn₂O₄) and lithium iron phosphate (LiFePO₄) are also commonly used cathode materials in solid-state Li-ion batteries.

1.1.3 Electrolytes

The electrolyte is a chemical medium that allows the movement of ions between the cathode and anode freely. The electrolyte for Li-ion batteries is a mixture of organic solvent and electrolyte salt compound. In conventional Li-ion batteries, usually liquid electrolytes have been used that is composed of a lithium salt (LiBF_4) in an organic solvent (ethylene carbonate). Since the commercialised liquid-based Li-ion batteries facing some safety issues, solid-state Li-ion batteries is one of the solutions that can overcome these safety issues in the battery. Solid-state Li-ion batteries using solid electrolyte materials that can reduce the risk of flammability of liquid electrolytes.

1.1.4 Mechanism of charge-discharge Li-ion Batteries

The charging and discharging mechanism of Li-ion batteries shows in Figure 1.2. Initially, the external energy will force the Li-ions to move out from the cathode and flow via solid electrolytes to intercalate at the anode. At the same time, the electrons will move around the external circuit during the charging process. All Li-ions are extracted out from the cathode where the de-intercalation process takes place and the intercalation process occurs at the anode. The battery is fully charged and ready to use when there is no more movement of Li-ions from cathode.

Then, during the discharging process, Li-ions will be deintercalated at the anode and move back through the solid electrolyte to intercalate at the cathode. As well as electrons also will migrate back from the anode to the cathode through external circuits powering up electronic devices such as mobile phones, laptop computers and digital

cameras. When all the Li-ions have moved back to the cathode, the battery is fully discharged and need to be recharge again. Hence, both positive and negative electrodes allow Li-ions to move in and out of the electrode with a process called intercalation (insertion) and de-intercalation (extraction).

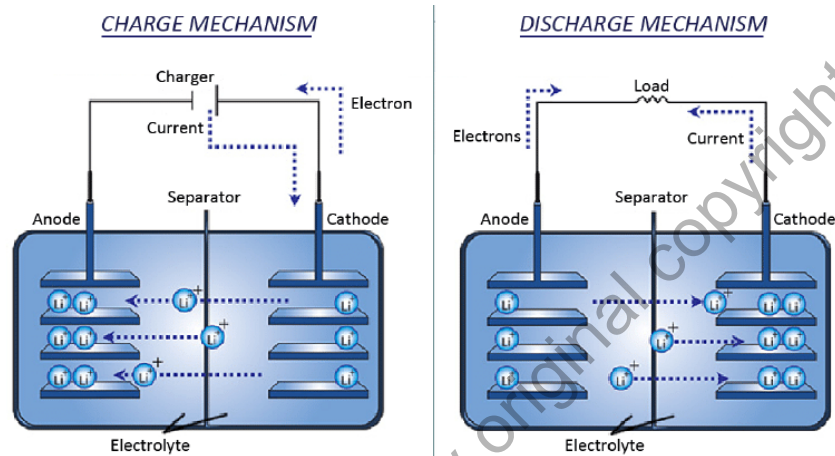


Figure 1.2 Charging and discharging mechanism of Li-ion batteries.

Current conventional Li-ion batteries usually consist of a liquid electrolyte which possesses limitations over its advantages. The chances of leakage of the electrolyte increase if any hole is present is one of the drawbacks of liquid electrolytes. Furthermore, the formation of dendrites Li in the liquid electrolyte battery make the battery is prone to an explosion (Kim et al., 2015). Since conventional batteries lack of safety, many researchers focused on creating new solid electrolytes rechargeable Li-ion batteries to meet the need for portable electronics.

All-solid-state Li-ion battery nowadays finds great potential applications in many energy conversion and storage device. Inorganic solid electrolytes play a major impact on the performance of the battery as they can effectively prevent explosive accidents that often happen in liquid electrolytes Li-ion batteries. The advantages of the solid-state

electrolytes are good thermal and chemical stability, high power and energy densities and especially good safety (Geng et al., 2016). Figure 1.3 shows the schematic diagram of conventional and solid-state Li-ion batteries. In this study, a composition of $\text{Li}_7\text{La}_3\text{Ce}_2\text{O}_{12}$ was proposed as a potential material for solid electrolytes. There is no evidence so far from our knowledge that intrinsic properties of $\text{Li}_7\text{La}_3\text{Ce}_2\text{O}_{12}$ been analysed in the literature. Therefore, we believed that this is the first scientific research been conducted to evaluate the crystallographic, electrical and microstructural properties of $\text{Li}_7\text{La}_3\text{Ce}_2\text{O}_{12}$.

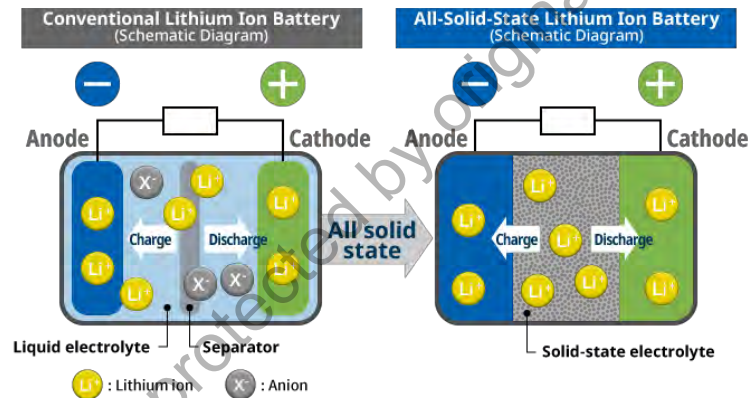


Figure 1.3 Schematic diagram of conventional and solid-state Li-ion batteries.

1.2 Problem statement

Solid electrolytes require high Li-ionic conductivity and good chemical stability. So far, the inorganic solid electrolytes with conductivities higher than $10^{-6} \text{ S cm}^{-1}$ at room temperature have been developed such as garnet-type structure $\text{Li}_7\text{La}_3\text{Zr}_2\text{O}_{12}$. However, many issues and challenges still exist that are faced by garnet-type structure $\text{Li}_7\text{La}_3\text{Zr}_2\text{O}_{12}$. The ionic conductivity is still lower than liquid electrolytes. In addition, the $\text{Li}_7\text{La}_3\text{Zr}_2\text{O}_{12}$ exhibit a polymorph structure that exists in a tetragonal and cubic phase where the

tetragonal phase ($10^{-6} \text{ S cm}^{-1}$) has low ionic conductivity while the cubic phase ($10^{-4} \text{ S cm}^{-1}$) was unstable at room temperature. The formation of pyrochlore $\text{La}_2\text{Zr}_2\text{O}_7$ during the synthesis of $\text{Li}_7\text{La}_3\text{Zr}_2\text{O}_{12}$ is also one of the challenges in synthesizing the pure phase of $\text{Li}_7\text{La}_3\text{Zr}_2\text{O}_{12}$. Thus, cerium (Ce^{4+}) is subject of interest in this study. The cerium is used to replace zirconium as it has relatively larger ionic radii compared to zirconium. The ionic radii for cerium and zirconium are 0.87 \AA and 0.72 \AA , respectively. There is a possibility that substituting Zr by Ce will resulting the expansion of garnet-type crystal structure. Therefore, it may allow Li-ions move easily within the crystal lattice and resulting relatively higher ionic conductivities in $\text{Li}_7\text{La}_3\text{Ce}_2\text{O}_{12}$ compared to $\text{Li}_7\text{La}_3\text{Zr}_2\text{O}_{12}$.

1.3 Research objectives

1. To evaluate crystallographic properties of $\text{Li}_7\text{La}_3\text{Ce}_2\text{O}_{12}$ as a garnet-type solid electrolyte synthesized by using conventional solid-state reaction method.
2. To investigate the structural and electrical properties of $\text{Li}_7\text{La}_3\text{Ce}_2\text{O}_{12}$ with different amount of lithium excess, different preparation method and the doping of Sn and Zr doped $\text{Li}_7\text{La}_3\text{Ce}_2\text{O}_{12}$.
3. To investigate the correlation between the structural, electrical and microstructural properties of $\text{Li}_7\text{La}_3\text{Ce}_2\text{O}_{12}$ with different amount of lithium excess, different processing methods and the doping of Sn and Zr doped $\text{Li}_7\text{La}_3\text{Ce}_2\text{O}_{12}$.

1.4 Scope of study

In this study, the effect on structure, electrical and microstructural properties of $\text{Li}_7\text{La}_3\text{Ce}_2\text{O}_{12}$ as solid electrolytes for rechargeable Li-ion batteries will be investigated. Initially, this study will be focusing on the synthesis of pure phase $\text{Li}_7\text{La}_3\text{Ce}_2\text{O}_{12}$ as garnet-type solid electrolytes by using the conventional solid state reaction method. Then, the effect of different amounts of lithium excess (10%-40%) on the structural and electrical properties is also intensively being studied. Furthermore, the effect of different synthesizing routes on the garnet-type structure $\text{Li}_7\text{La}_3\text{Ce}_2\text{O}_{12}$ samples was investigated by using the planetary ball-mill method. The characterization techniques involved in this project are X-ray Diffraction (XRD), Impedance spectroscopy and Scanning Electron Microscopy (SEM). Therefore, the properties of the $\text{Li}_7\text{La}_3\text{Ce}_2\text{O}_{12}$ were correlated to one another with the effect of lithium excess and the processing method of $\text{Li}_7\text{La}_3\text{Ce}_2\text{O}_{12}$ can be concluded.

1.5 Thesis structure

This thesis is divided into several chapters which cover various aspects of the research. This includes the variety of testing to perform this study. Chapter 1 present the introduction for the research title, objectives and problem solving which will provide readers with a brief review and significance of the study. Chapter 2 deals with a literature review including the development and synthesizing method used to investigate these solid electrolyte materials. Chapter 3 focuses on the details of the materials used, the method of synthesizing single phase garnet-type structure $\text{Li}_7\text{La}_3\text{Ce}_2\text{O}_{12}$ and characterization techniques of the sample. Chapter 4 specifically discusses the results obtained from